CCS Chemistry

IMMEDIATE ONLINE ACCEPTED (IOA) ARTICLE

IOA Posting Date: May 13, 2024

TITLE: Flexible Organic Crystals for Light Delivery in Biological Tissues

AUTHORS: Linfeng Lan, Xiuhong Pan, Patrick Commins, Liang Li, Luca Catalano, Dongmei Yan, Haonan Xiong, Chenguang Wang, Panče Naumov, Hongyu Zhang

DOI: 10.31635/ccschem.024.202404188

CITE THIS: *CCS Chem.* **2024**, Just Accepted. DOI: 10.31635/ccschem.024.202404188

Flexible Organic Crystals for Light Delivery in Biological Tissues

Linfeng Lan,[1] Xiuhong Pan,[1] Patrick Commins,[2] Liang Li,[2,3] Luca Catalano,[4] Dongmei Yan,[5] Haonan Xiong,[6] Chenguang Wang,[6]* Panče Naumov,[2,7,8,9]* Hongyu Zhang[1]*

[1]State Key Laboratory of Supramolecular Structure and Materials, College of Chemistry, Jilin University, Changchun, 130012

[2]Smart Materials Lab, New York University Abu Dhabi, PO Box 129188, Abu Dhabi

[3]Department of Sciences and Engineering, Sorbonne University Abu Dhabi, PO Box 38044, Abu Dhabi

[4]Laboratoire de Chimie des Polymères, Université libre de Bruxelles (ULB), 1050, Brussels

[5]Department of Immunology, College of Basic Medical Sciences, Jilin University, Changchun, 130012

[6]State Key Laboratory of Integrated Optoelectronics, Key Laboratory of Advanced Gas Sensors of Jilin Province, College of Electronic Science and Engineering, Jilin University, Changchun, 130012

[7]Center for Smart Engineering Materials, New York University Abu Dhabi, PO Box 129188, Abu Dhabi

[8]Research Center for Environment and Materials, Macedonian Academy of Sciences and Arts, Bul. Krste Misirkov 2, MK–1000 Skopje

[9]Molecular Design Institute, Department of Chemistry, New York University, 100 Washington Square East, New York, NY 10003

*Corresponding Author(s): wangchenguang@jlu.edu.cn; pance.naumov@nyu.edu; hongyuzhang@jlu.edu.cn

Abstract

Optically transmissive materials are indispensable for the transmission of light or light-encoded signals in telecommunications and optobiomedical techniques. Here, we propose that slender crystals of small organic molecules can be used as optically transparent, flexible, lightweight, and emissive media to deliver photons into or through biological tissues as an alternative to silica- or polymer-based light waveguides. We demonstrate that organic crystals remain transmissive in various porcine tissues, and their efficiency in light transduction depends on the intrinsic optical properties of the crystal, optical path, geometry of excitation,

and the type of tissue. Moreover, elastically or plastically deformable organic crystals remain mechanically compliant and can be bent after they have been embedded in the tissue, opening prospects for designing a new class of biocompatible light waveguiding elements based on crystalline organic materials. In vivo implantation and toxicity assays capitalize on mechanical flexibility and biocompatibility in animal models. Within a broader context, the high transparency, anisotropy, and biocompatibility of some organic crystals turn this emerging class of materials into a prospective platform for delivering photons for specific interaction with target cells in tissues for applications such as photodynamic therapy and optogenetics.

Keywords

organic crystals, mechanically flexibility, optical waveguides, biocompatibility, light transmission *in vivo*

Introduction

Interaction of biological tissues with light, whether it is for the purpose of harnessing natural light such as that by some deep-water organisms like sponges,[1,2] integration of soft robotic or prosthetic systems,[3,4] or clinical applications such as photodynamic therapy and optogenomics,[5–7] requires transduction of light from the source or point of entry to the target for excitation via an optically transmissive medium. The common optical waveguides that are currently used for such purposes in nature or clinical practice are based on biogenic or processed silica. However, the nascent brittleness and rigidity of this rather accessible material stand in stark contrast with the pronounced softness of the target biological tissues; when mishandled or being used in contact with tissues over a prolonged time, silica-based fibers could mechanically damage cells of softer tissues, or even trigger inflammation processes.[8,9] Polymer-based optical waveguides could potentially circumvent this shortcoming, and, being more compatible with biological interfaces,[10–12] optically translucent polymers were thought to hold prospects for organic wearables and implantable optical sensors. The polymeric materials that can be used to that end, however, are inevitably amorphous and structurally isotropic. Increased crystallinity of the polymer—for example by thermal treatment, mechanical damage or aging—results in enhanced light

scattering from the ensuing crystalline domains, rendering these materials opaque and ultimately decreasing their optical transparency. These issues call for alternative optical waveguiding materials that are light, soft, biocompatible, and mechanically compliant. In addition to the usual light transduction by total reflection, the candidate materials should also be capable of advanced modes of light-cell interactions, such as direction-specific modulation of light intensity or non-linear optical effects.

Being transparent, light-weight, and in many cases, colorless, organic crystals have been recently established as a distinct materials class that provides an optically transducive medium that readily guides visible radiation by multiple total internal reflection.[13–18] Beyond the visible range, organic crystals of simple compounds have also been suggested recently for transduction of light signals in the near-infrared (telecom) regime, where the entirety of the Internet traffic is currently conducted.[19] Being composed of only light atoms, organic crystals have low density. They also are light in weight, and in some instances when they are made of natural constituents, are also known to be biocompatible.[20] Their chemical structures can be varied by relatively simple chemical/crystallization procedures, and unlike silica for which the sole access to chemically different compositions relies on doping with other elements such as germanium, the chemical versatility of organic crystals offers access to a great diversity in physical, mechanical, and optical properties. With the advent of mechanically compliant organic crystals and the rise of adaptive crystals within the realm of the "crystal adaptronics", one of the main obstacles that had impeded wider application of molecular organic crystals—the lack of mechanical robustness due to fragility and brittleness—has been overcome.[21–24] It is surprising that organic crystals have been seldom interfaced with applications in biological tissues, and almost no biological toxicity has been measured. In this attempt aimed at introduction of organic crystals as potential light transducers in tissues and living organisms, we explore the physical aspects of their performance both *in vitro* and *in vivo*, and we set the basis for their future implementation as mechanically compliant optical waveguides that can be used to transduce light onto or through biological materials.

Experimental Methods

1. Preparation and general characterization. The synthesis and crystal growth of compounds **O**, **G**, **B** and **P** were performed according to procedures reported in the literature.[25–28] Weak ultraviolet light for excitation was generated with a 365 nm or 375 nm optical source and passed through an optical fiber. The UV−vis absorption spectra were recorded by using a Shimadzu UV-2550 spectrophotometer. The emission spectra were recorded with a Maya2000 Pro CCD spectrometer. Three-point bending tests were carried out by using an Instron 5944 universal testing system with a capacity of 5 N Instron 2530 load cell. The nanoindentation measurements were conducted with Agilent Nano Indenter G200 with the CSM method and an XP-style actuator. The widths and thicknesses of the crystals were observed with an Olympus BX61 microscope.

2. Optical waveguiding tests. For the optical waveguiding tests, the crystal was irradiated by the third harmonic (355 nm) of a Nd:YAG (yttrium aluminum garnet) laser with a pulse duration of about 5 ns. The energy of the laser was adjusted by using calibrated neutral density filters. The beam was focused onto a strip whose shape was adjusted to 3.3 × 0.6 mm by using a cylindrical lens and a slit. The emission was detected at one end of the crystal by using a Maya2000 Pro CCD spectrometer. The crystal was placed on a silicon wafer, and one tip of the crystal extended out of the edge of the wafer to align it with the probe of the spectrometer. While changing the irradiation locations, spectral data were collected for each location at the excitation site and at the tip of the crystal. After the collection, the crystal was bent and fixed with glue, and the data was collected by using the aforementioned method. The optical loss coefficients (α) were obtained by a single exponential fitting of the function $I_{tip} / I_{body} = A \exp(-\alpha D)$, where I_{tip} and I_{body} are the fluorescence intensities of out-coupled and incidence light, and D is the distance between the excited site and the tip where the emission was collected.

3. Cell culture and cytotoxicity assay

Cell culture. In general, the Hela cells were cultured in Dulbecco's modified Eagle's medium (DMEM, high glucose, pyruvate) containing 10% fetal bovine serum (FBS) and 1% Antibiotic-Antimycotic (AA) at 37 °C in a humidified 5% (vol/vol) CO_2 incubator.

Cytotoxicity assay. The effect of crystals **O**, **B** and **P** on cell viability was analyzed by using 3-(4,5-dimethylthiazol-2-yl)-2,5-diphenyltetrazolium bromide (MTT). Cells were seeded into a flat-bottomed 96-well plate (1 x 10^4 cells/well) and incubated in DMEM containing 10% FBS (DMEM+) at 37 °C in a 5% CO_2 incubator for 24 h. The medium was then replaced with a culture medium DMEM+ containing various concentrations of **O**, **B** and **P** (0, 0.5, 1.0, 2.0, 5.0 and 10.0 uM) and 1% DMSO. After incubation for 24 h, MTT reagent (final concentration, 0.5 mg/mL) was added to each well, and the plates were incubated for another 4 h in a CO_2 incubator. Excess MTT tetrazolium solution was then removed. After the formazan crystals were solubilized in DMSO (100 uL/well) for 30 min at room temperature, the absorbance of each well was measured by a microplate reader (Bio-Tek Instruments, Inc) with an excitation at 490 nm.

4. Animal ethics and histological examination

Animal ethics. The experiment was performed with approval from the Animal Care and Ethics Committee of Jilin University in China. All experiments were performed according to the Care and Use of Laboratory Animals published by the US National Institutes of Health (NIH Publication, 8th Edition, 2011).

Histological examination. Balb/c mice (*n* = 5 for each group) were intravenously injected with crystals **P** (100 μL /10 mg, 10 μM in 95% PBS and 5% DMSO), and major organs including brain, lung, kidney, liver, spleen, and heart were collected, fixed and stained with hematoxylin and eosin (H&E) after 24 h administration. The control group was treated with 100 μL / 10 mg of 95% PBS and 5% DMSO. The tissue images were taken by a converted Nikon microscope with a 20× objective.

Results and Discussion

To assess the performance of crystals as active waveguides in biological tissues, we selected three previously reported and, intentionally, chemically unrelated organic crystals, (*Z*)-3-(furan-2-yl)-2-(4-(((*E*)-2-hydroxy-5-methylbenzylidene)amino)phenyl)acrylonitrile (**O**), 9-anthracenecarbonitrile (**G**) and (*Z*)-4-(2-cyano-2-(4-(trifluoromethoxy)phenyl)vinyl)benzonitrile (**B**) (Figure 1a; Supporting Information Figure S1).[25–27] Crystals of

another compound, 2,2′-((1*E*,1′*E*)-1,4-phenylenebis(ethene-2,1-diyl))dibenzonitrile (**P**), were selected for additional *in vivo* experiments (see below).[28] When excited with UV light, crystals of **O**, **G**, and **B** conveniently emit fluorescence—orange-red, green and blue, respectively, a property that provides the opportunity to examine the transmission of light at different wavelengths (Supporting Information Figure S1). Their solid-state absorption and emission spectra show that their active and passive light-waveguiding properties depend on the wavelength of the light source (Figure 1b; Supporting Information Figure S2). If they are excited with a 355 nm laser, these crystals act as *active* waveguides by emitting fluorescence of different colors (Figure 1c–e and 1i). Instead, when a 654 nm laser light is used for excitation, they act as *passive* waveguides by transmitting the input signal with an unaltered spectrum (Figure 1f–h, j). The mechanical properties of the crystals were elucidated from the correlation between the stress and strain or between the load and displacement in three-point bending tests (Supporting Information Figure S3; Supporting Information Table S1). While needle-like crystals of **O** and **B** are elastic under external force and regain their bent shape, crystals of **G** are plastic and remain bent after they have been deformed. The Young's moduli and hardnesses of the crystals were determined by nanoindentation, and the results are summarized in Supporting Information Figure S4 and Supporting Information Table S2.

We first qualitatively evaluated the ability of the crystals to transmit light signals through biological tissues. The experiments were performed with two slabs of porcine tissue (**PT**) that were *ca.* 15 mm long and 1–2 mm thick. After removing the skin, the porcine tissue was cut into thin slices of both adipose (fat) and lean muscle tissue. When irradiated laterally, the tissue was strongly absorbing, and the 654 nm laser light could penetrate only 4.60 mm under its surface, while the 365 nm UV light could only penetrate 2.65 mm (Figure 1k, m). A single crystal of **O** (sample **O1**) was then sandwiched between the two tissue slabs, and weak ultraviolet light was applied to facilitate the observation of the crystal via its emission. For simplicity of the measurement, the light excitation was applied onto the tissue above the crystal and collected at the end of the crystal. The embedded

crystal **O1@PT** was capable of passive and active transmission of light across a distance of 16.02 mm without significant attenuation compared to the porcine tissue (Figure 1l, n). To confirm reproducibility, the results obtained with a second crystal of **O** (**O2@PT**) embedded in tissue were consistent with those for **O1@PT**, with a penetration depth of the pristine pork tissue of 3.54 mm at 654 nm and 2.20 mm at 365 nm (Supporting Information Figure S5). The same experiments were carried out with crystals of **G** and **B** (**G@PT** and **B@PT**, respectively), and they were found also to be capable of transmitting both active and passive light signals in the tissue across distances of up to 25.81 and 36.85 mm, respectively (Supporting Information Figures S6 and S7). To test the mechanical flexibility of the embedded crystal **O1@PT**, the crystal was bent, and it did not fracture (Figure 1o–q). The retention of mechanical compliance demonstrates that organic crystals, in principle, fulfill one of the key prerequisites for flexible biomedical waveguides. We further confirmed that not only elastic and plastic organic crystals retain their mechanical properties when they are embedded in tissues, but they can also be bent multiple times. This result provides further support for these materials as flexible biocompatible optoelectronic light transducers. Moreover, when a crystal of **B** with a length of about 4 cm is embedded in the tissue, the signal can be well transmitted to the other end regardless of whether the 654 nm light was shone vertically or parallel to the longest crystal direction (Figure 1r, s).

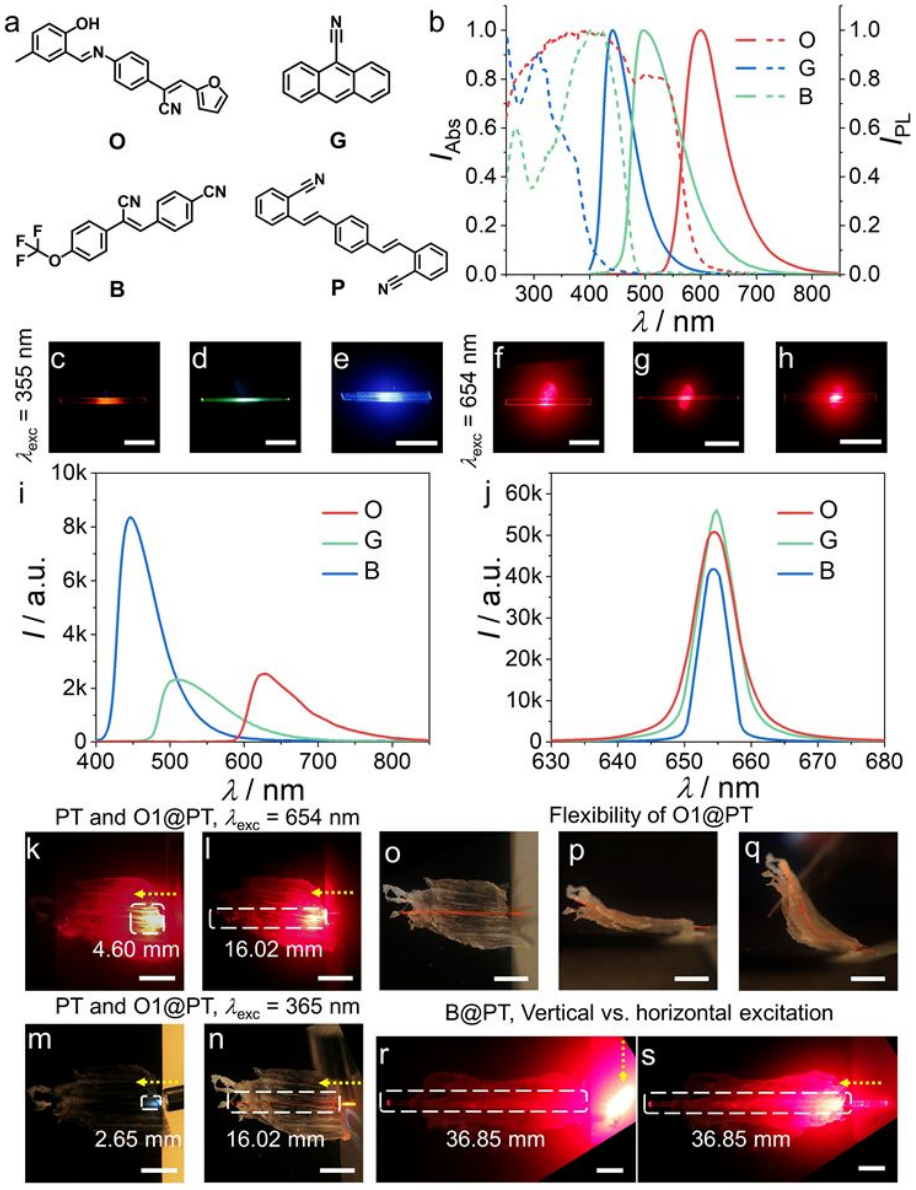

Figure 1 | ***Chemical structures, appearance, and emission of organic crystals for delivery of light to porcine tissues.*** *(a) Chemical structure of compounds* ***O***, ***G*** *and* ***B****. (b) Normalized absorption (broken line) and fluorescence emission spectra (solid line) of crystals of* ***O***, ***G*** *and* ***B****. (c–h) Photographs of crystals of* ***O***, ***G*** *and* ***B*** *under a 355 nm laser irradiation (c–e) and 654 nm laser irradiation (f–h). (i, j) Spectra collected at the tip of crystals of* ***O***, ***G*** *and* ***B*** *as their other end is excited with a 355 nm laser (i) or 654 nm laser (j), respectively. Panel i shows the fluorescence, while panel j shows a spectrum identical to that of the incident light. (k–n)*

*Photographs of the light in porcine tissue (thickness ~2 mm) taken before (k, m) and after (l, n) insertion of the crystal **O** waveguide. In panels k and l, an external light source (654 nm laser) was directly applied to the surface of the tissue (k), and then coupled to a crystalline waveguide implanted into the tissue (l). In panels m and n, an external (365 nm) UV light was directly applied to the surface of the tissue (m), and then coupled to a waveguide implanted into the tissue (n). (o–q) Mechanical bending of a crystal of **O** in porcine tissue, **O1@PT**. (r, s) Photographs of **B@PT** excited with a 654 nm laser perpendicular (r) to and parallel (s) to the direction of light transmission. The dotted yellow arrows indicate the direction of the laser: the horizontal arrows represent laser light parallel to the direction of light transmission, and the vertical arrows represent laser light perpendicular to the direction of light transmission. The length of the scale bars on all panels is 5 mm.*

To quantify the transmission capability, we determined the optical loss coefficients (OLCs) of crystals embedded in the tissue. Unembedded crystals of **O**, **G** and **B** were first irradiated in air at different positions with a 355 nm pulsed laser, and the emission intensity was measured at one of their ends (Figure 2a–c). The intensity decreased as the distance between the points of excitation and measurement increased. The measurement was repeated after embedding the crystals in the tissue (Figure 2d). Different crystals of the same compound (as an example, the spectra of two crystals of **B** are shown in Figure 2e) were used to confirm reproducibility. The optical loss coefficients (OLCs) of the original crystals **O**, **G** and **B**, and crystals embedded in tissue **O**–**B@PT** were calculated by fitting the resulting data according to the literature method[29] as shown in Figure 2f–h. Expectedly, the transparency decreases and the OLC increases when the crystals are incorporated into the tissue (Figure 2d, e). As typical values, α for a crystal of **O** at 613 nm was found to be 0.186 mm^{-1} in air and 0.250 mm^{-1} in the tissue (Figure 2f). These results confirm that the tissue attenuates light strongly, as expected from the higher refractive index of porcine tissue (ca. 1.38 – 1.41)[11] compared to air (~1), which effectively increases the overall OLC. We note that additional losses are expected from scattering at the interface between the crystal and the tissue. The values of α were wavelength-dependent, so for a crystal of **G** at 412 nm, 437 nm and 496 nm, α was determined to be 0.460, 0.394 and 0.200 mm^{-1} in air, and 0.542,

0.516 and 0.253 mm^{-1} in tissue (Figure 2g). Finally, while the OLC is quite consistent for different neat crystals, its value depends on the optical path through the tissue, and therefore for the same crystal, it might be slightly different when it is embedded in different tissue samples, even if they are of the same type (Figure 2e, h).

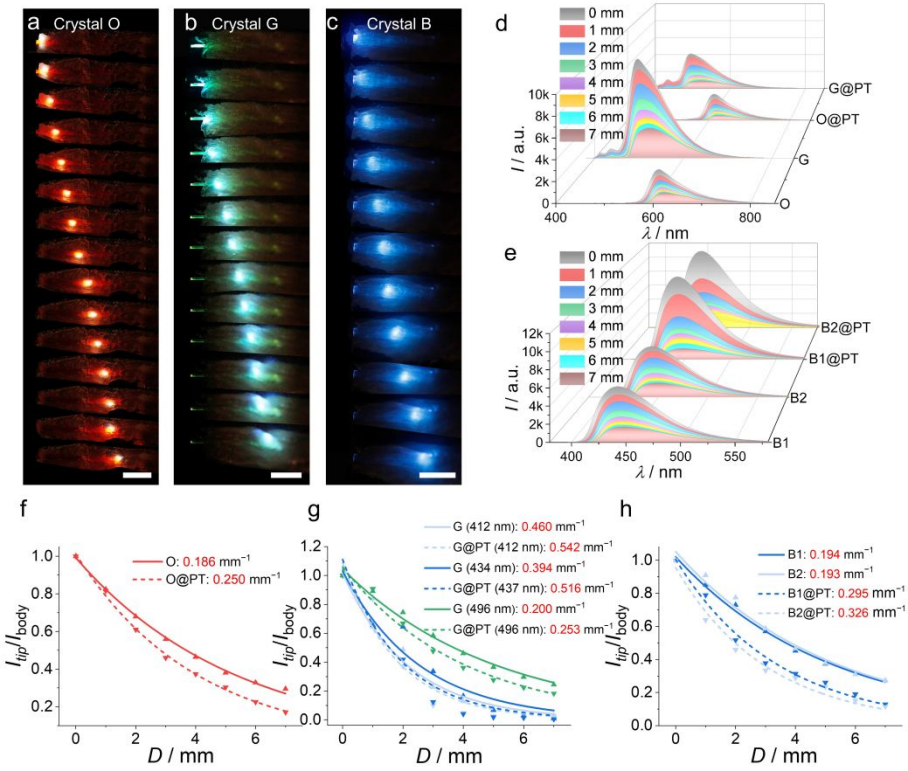

Figure 2 | ***Optical transmission capability of organic crystals through biological tissues.*** *(a–c) Images of organic crystals embedded in porcine tissue (**O–B@PT**) and excited with UV light. Crystals of **O**, **G** and **B** were sandwiched between tissue slices and excited with a 355 nm laser focused at different positions, whereby they emitted light with different colors. (d, e) Fluorescence spectra collected at the tip of the crystal of **O–B** alone (**O–B**) and in porcine tissue (**O–B@PT**) with different distances between the tip and the excitation site of the laser. Two samples of **B** (**B1** and **B2**) were measured for both the **B** and **B@PT** to confirm reproducibility. (f–h) I_{tip}/I_{body} decays of nascent crystals **O–B** and after incorporation in port tissue, **O–B@PT**. All scale bars are 5 mm.*

The experiments were repeated by using other types of porcine tissues (adipose and lean muscle tissues, Figure 3a, b, e, f) and with different geometries of irradiation of the crystal (Figure 3c, d, g, h). A selection of the results is summarized in Figure 3, and more results are available from the Supporting Information. Compared to vertical excitation (perpendicular to the crystal), horizontal excitation (parallel to the crystal) delivers more photons into the crystal, and thus the output signal intensity is consistently stronger, provided that the other conditions are maintained constant (Figure 3c, d, g, h, i). In addition to the thinly sliced pork tissue that includes both adipose and lean muscle (**PT**), soft adipose (**PF**) and hard lean (**PL**) cuts were also used (Figure 3i, j). Based on comparison of the output spectra and the OLCs we conclude that while the results between different crystals of the same compound vary only slightly due to the uniform composition of the crystals, the type of tissue has a strong effect on the light transmission. The overall light transduction is a result of the cumulative effectors of the transmission through both the crystal and the tissue, where the optical properties of the latter vary with its composition and thickness. The effect is additionally directly related to the inherent energy distribution of the incoming light, that is, the fluorescence spectrum of the crystal (Figure 3k).

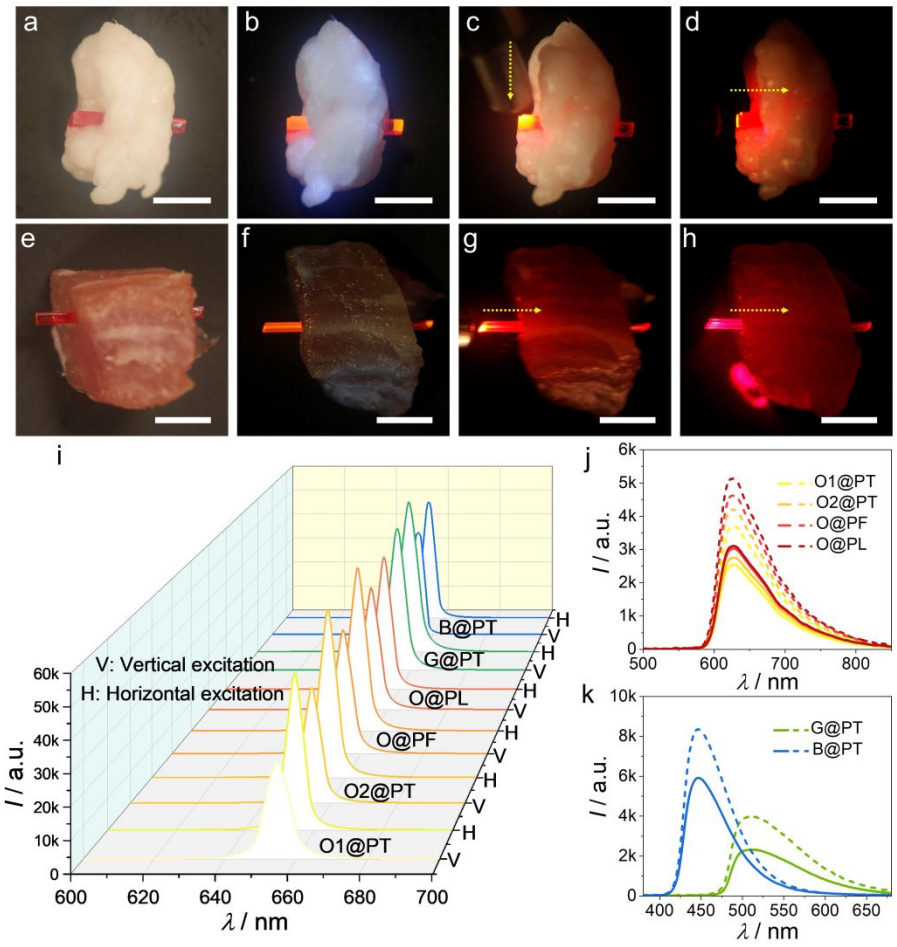

Figure 3 | ***Effect of the type of tissue on the transmission.*** *(a, b) Photographs of the crystal **O** inserted into porcine adipose (fat) tissue, **PF** (**O@PF**) in daylight (a) and under UV light (b). (c, d) The **O@PF** excited with a 365 nm UV light perpendicular (c) and parallel (d) to the direction of light transmission. (e, f) Photographs of the crystal **O** inserted into a lean muscle porcine tissue, **PL** (**O@PL**) in daylight (e) and under UV light (f). (g, h) The **O@PL** was excited with a 365 nm UV light (g) and 654 nm laser (h) parallel to the direction of light transmission. The dotted yellow arrows indicate the direction of the laser. All scale bars are 5 mm. (i) The corresponding spectra collected at the tip of **O1@PT**, **O2@PT**, **O@PF**, **O@PL**, **G@PT** and **B@PT** as their other ends were excited with a 654 nm laser along different directions, respectively. (j, k) The corresponding fluorescence spectra collected at the tip of **O1@PT**, **O2@PT**, **O@PF**, **O@PL**, **G@PT** and **B@PT** as their other*

ends were excited with a 365 nm UV light along different directions. Solid and dashed lines represent vertical and horizontal irradiation, respectively.

Encouraged by the results, we investigated the application of organic crystals as light transducers *in vivo*. Since these crystals are generally soft, their implantation required development of a method for insertion of the crystal into the tissue without damage. The implantation procedure was optimized by using chicken tissue. As shown in Figure 4a, the crystal was first placed in a needle of a syringe filled with Phosphate Buffered Saline (PBS), and the needle was slowly inserted into the tissue to a certain depth. A small segment of the needle was subsequently pulled out, and PBS was injected to exert force which pushed the crystal into the tissue. Finally, the syringe was slowly retracted, leaving one portion of the crystal embedded in the tissue, while the other portion remained exposed to air (Supporting Information Movie S1). By using this procedure, a crystal of **O** measuring 2.0 cm in length was inserted to a depth of 1.1 cm into the tissue, and approximately 1 mm away from the surface (Supporting Information Figure S8). When illuminated with a 365 nm light perpendicular to its length, the entire portion of the crystal that was embedded in the tissue emitted bright orange light (Supporting Information Figure S8b). However, when ultraviolet light was shone onto the crystal parallel to its length, only about 50% of the portion of the crystal embedded in the tissue emitted light (Supporting Information Figure S8b). Using the same method, a deformable crystal of **B** with a length of 1.9 cm was embedded into the tissue to a depth of approximately 0.9 cm and about 2 mm from the tissue's surface (Figure 4b). When one end of the crystal was excited, emission of blue light was observed from the tip of the crystal both in air and in the tissue (Figure 4c). We also confirmed that these crystals can be removed from the tissue without breaking (Supporting Information Movie S2).

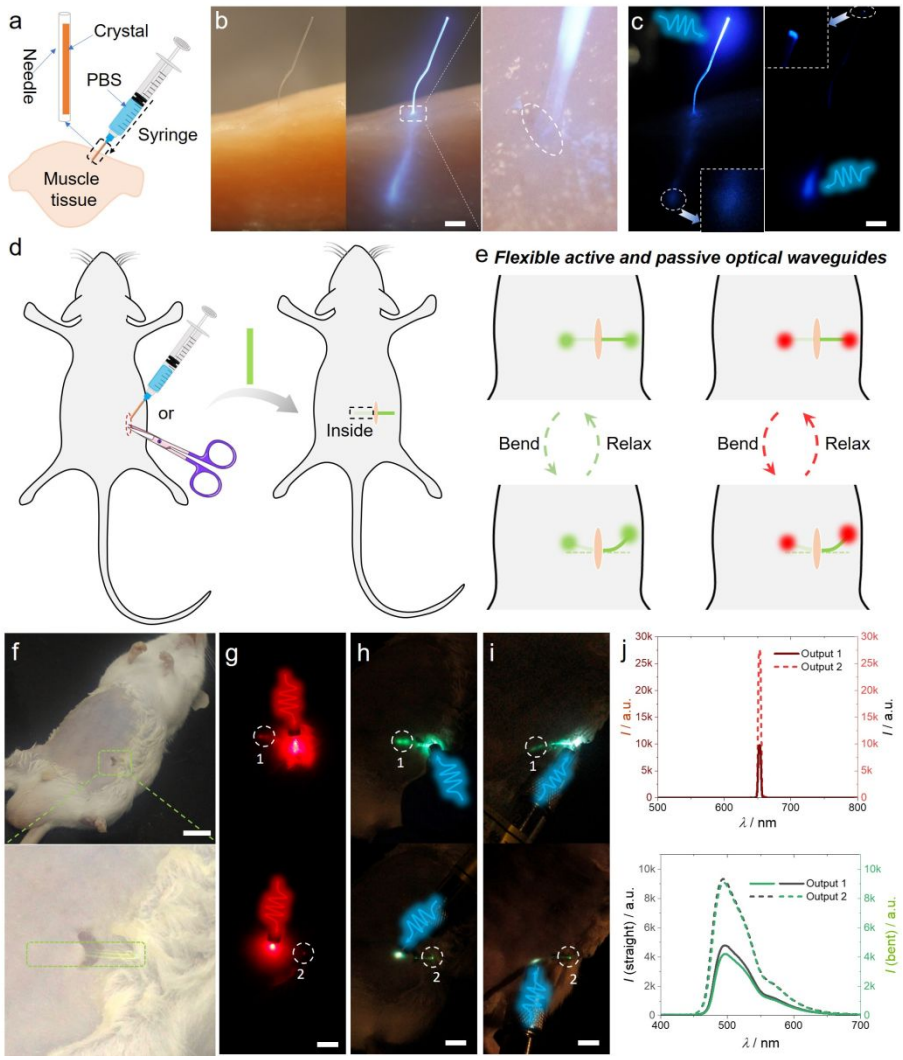

Figure 4 | ***Light transmission through flexible organic crystals in vivo.*** *(a) An illustration of the procedure used to insert a crystal into muscle tissue by using a syringe. (b) Photographs of a deformable crystal* ***B*** *embedded in chicken tissue in daylight (left) and under UV light (right). The rightmost panel shows a zoomed image of the perforation. (c) Optical waveguiding properties of a crystal of* ***B*** *embedded in a tissue. (d, e) Schematic illustration of the procedure for embedding a crystal in a mouse (d), and flexible active and passive optical waveguiding of light through the straight and bent crystal (e). (f) Photograph of a crystal* ***P*** *partially embedded under the abdominal epidermis of the anesthetized mouse. The lower panel shows a zoomed representation of perforation. (g) Passive optical waveguiding of light through a crystal* ***P*** *embedded in a mouse. (h, i) Active*

*optical waveguiding of light through a crystal **P** embedded in the mouse in straight and bent states. (j) The corresponding fluorescence spectra collected at the tip of the crystal **P** as its opposite end was excited with a 375 nm (bottom) or 654 nm (top) light. Output 1 is in the body and output 2 is in the air. The lengths of the scale bars are 2 mm in panels b and c, 1 cm in panel f, and 5 mm in panels g–i.*

With the insertion technique at hand, crystals of 2,2′-((1*E*,1′*E*)-1,4-phenylenebis(ethene-2,1-diyl))dibenzonitrile (**P**), which are known to be flexible (Supporting Information Figure S9), were embedded under the epidermis of a mouse, either with a syringe as described above (Figure 4d). After the mouse was anesthetized, its abdominal area was depilated, and a small incision was made under the abdominal epidermis. A 9 mm-long crystal of **P** was inserted completely under the epidermis (Supporting Information Figure S10a). Either 375 nm or 654 nm light source was used to excite one end of the crystal through the skin, and green and red fluorescence was observed at its other end respectively (Supporting Information Figure S10b, c). Similarly, an 8 mm-long crystal was inserted under the epidermis of a mouse up to about half its length (Figure 4f). In this case, the crystal was capable of both passive and active optical waveguiding, and in both straight and bent states, allowing for signal transmission from the air to the abdomen of the mouse, and vice versa (Figure 4e and 4g–i). We note that the section of the crystal that was under the mouse's skin had to be bent to be able to penetrate deeper into the interior, which resulted in a slight decrease in intensity of the collected light (Figure 4j). To further validate the mechanical stability of the crystal as optical waveguide within the living organism, a portion (6 mm) of a 1.6 cm crystal **P** was inserted into the subcutaneous tissue of a mouse using a syringe, as described above. The crystal was then strongly and repeatedly bent (Supporting Information Figure S11). As shown in Figure 5a and 5b, during bending of the crystal 30 times and excitation of its aerial terminus with a 375 nm light, bright and stable green light signal was consistently observed within the mouse's body. This result confirms the notable mechanical compliance of the crystal which sustains delivery of photons *in vivo*, even upon mechanical deformation. Additionally, to eliminate the possibility of diffraction of the incident light, 375

nm or 654 nm light sources were placed in four dispositions relative to the crystal, and the crystal embedded in the mouse did not exhibit any emission (Supporting Information Figure S12).

One of the main prerequisites for application of these materials in practice is their potential biological toxicity. Although this property is naturally specific to the particular compound used and could vary across different organic crystals that could be used as optical waveguides, here we assessed the cytotoxicity of **O**, **B** and **P** toward cancerous HeLa cells by using the MTT method (for details, see the Supporting Information). Crystals of **G** could not be assessed due to their partial dissolution in the tissue. As shown in Figure 5c, the cell viabilities after 24 h of incubation with **O** and **P** at various concentrations, even at a very high concentration of 10 μM L^{-1}, were over 91% and 99%, respectively, demonstrating good biocompatibility of **O** and **P**. Compound **B** showed good biocompatibility for cells when its concentration was lower than 2 μM L^{-1}, however the relative cell viabilities were 68% and 64% at concentrations of 5 and 10 μM L^{-1}, respectively.

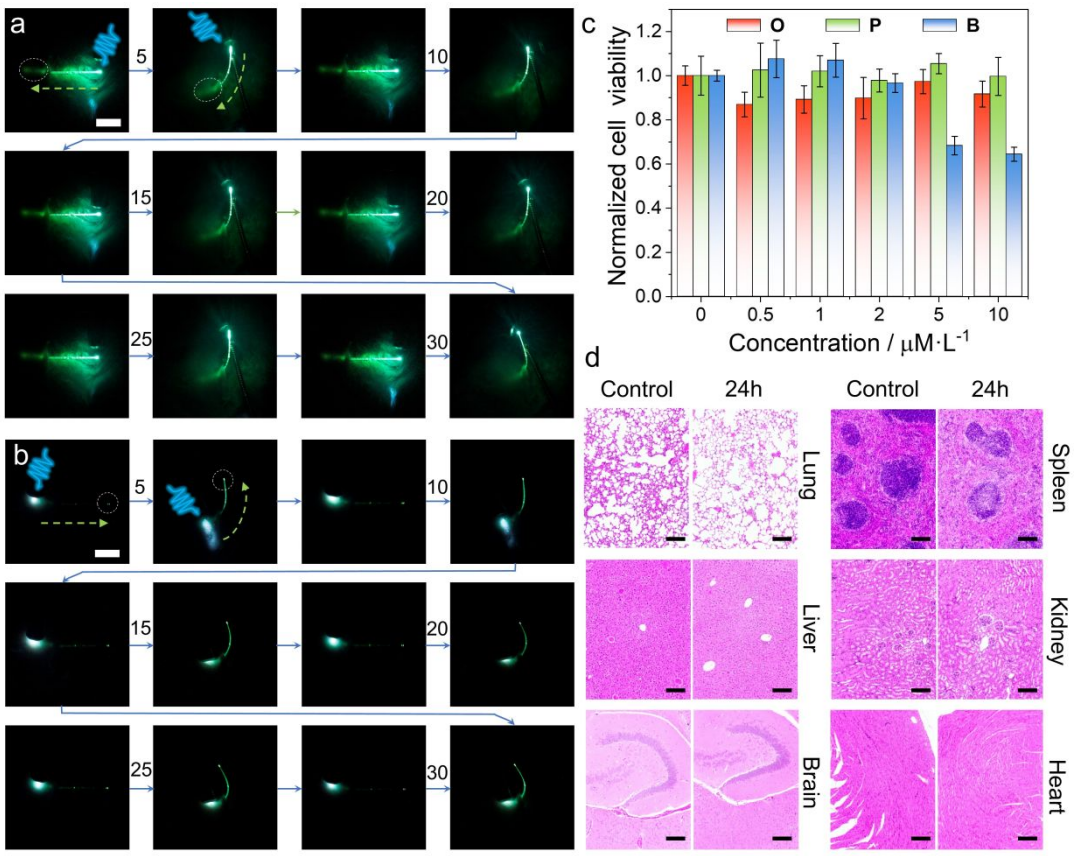

Figure 5 | ***Mechanical stability of the organic crystals embedded in mouse and assessment of their cytotoxicity.*** *(a,b) Optical waveguiding of a crystal of **P** which was bent 30 times. The aerial (a) and implanted end (b) of the crystal in the mouse were excited by a 375 nm UV light after every 5 bending cycles. The lengths of the scale bars are 5 mm in panels a and b. (c) Cell viability results of the HeLa cells incubated with the compounds **O**, **P** and **B** assessed by an MTT assay. The results are expressed as percentages of the probe-free controls. All data are presented as mean ± s.d. (n = 10). (d) H&E stained photomicrographs of tissue slices (lung, liver, brain, spleen, kidney and heart) of mice injected with crystals **P** at a dose of 100 µL / 10 mg per time. The lengths of all scale bars are 100 µm.*

Moreover, the *in vivo* toxicity of **P** was investigated by histological examination of the major organs of a treated mouse. After intravenous injection of **P** (100 µL / 10 mg, 100 µM L^{-1} in 95% PBS and 5% DMSO) for 24 h, the major organs, including brain, lung, heart, liver, kidney, and spleen, were excised and stained with hematoxylin and eosin (H&E). As displayed in Figure 5d, no obvious abnormalities or inflammations were observed in the tested organs, suggesting negligible *in vivo* toxicity of **P**. The above results confirmed that these and possibly other flexible organic crystals, especially when they are composed of non-toxic molecules,[30] can be used as biocompatible organic optical fibers for biological applications.

To further assess the performance of the organic crystals as optical waveguides for biomedical applications, we performed extensive literature search and analysis of refractive indices, OLC values, and mechanical properties (Young's moduli and elongation thresholds) reported for organic crystals (for details, see the Supporting Information Methods). These parameters were then compared to those of the reported values for artificial polymer waveguides or natural light-transmitting materials (Table 1). Direct comparison of OLCs proved to be a challenging task, considering that it has been recently demonstrated that the size can affect the optical loss,[31] and some organic crystals in the literature were characterized at a micrometer-size, while the

size of others was on the order of centimeters. As shown in Supporting Information Table S3, the OLCs of organic crystals with lengths above millimeters are mostly in the range of 0–1 mm^{-1}, while those of micrometer lengths are in the range of 1.0 and 457 mm^{-1}. In general, organic crystals possess mechanical and optical properties that challenge the performances of their polymeric counterparts. Indeed, the soft mechanical properties of these prototypical waveguides, comparable to polymers employed in biophotonic devices (Table 1), turn them into ideal candidates to overcome the mechanical mismatch between the most widely used silica-based optical fibers and biological tissues. Unlike silica and polymeric materials, molecular single crystals possess superior structural characteristics, and specifically long-range order, tunable dimensionality (1D, 2D and bulk 3D highly ordered structures),[32–34] and when they are of good quality, they are also devoid of grain boundaries and other defects. Among the features that are favorable for waveguiding materials, they have low OLCs, high refractive indices, broad emissive range that extends from UV to the near-IR range,[19,35] and the possibility for both active and passive light transport in luminescent π-conjugated systems.[36] In addition to mechanical flexibility, which has been studied by using standard techniques,[37] certain organic crystals are known to exhibit shape-memory effect,[38] self-healing[39] and even rapid ballistic processes for disintegration—exotic properties that could be used to disrupt optical or electronic circuits.[40–44] Other, more specific advantages of molecular single crystals over the silica-based waveguides are their capability of optical filtering,[19,45] light modulation,[46] photomechanical response,[47] bio-based design,[19,48,49] crack-repairing ability,[45] logic gate operations,[16,28] chiro-optical signaling,[50,51] and lasing.[28,52]

Table 1. Mechanical and optical properties of polymeric biomaterials that have been used for biocompatible waveguides and the respective values for organic crystals

Material	Refractive index	Optical loss [dB cm^{-1}]	Young's modulus	Maximum elongation [%]
Organic crystals	~ 1.6[53]	0.4–4570 (cm^{-1})[54,55]	1–25 GPa[56]	20[56–58]
Silkworm silk	1.54–1.55	0.1–28	3.8–17 GPa	4–33.3
Spider silk	1.5–1.7	0.7–11	1–24 GPa	4–30
Agarose gels, alginate gels, gelatins	1.34–1.54	0.3–13	30–80 kPa	700–2000
Cellulose	1.475	0.1	–	20–70
Chitosan	1.38–1.54	0.8–7.3	1.3 GPa	3
PLA, PLLA, PDLA	1.46–1.47	1.5	2.7–7 GPa	3–100 (non-elastic)
PGA	1.45–1.51		6.5 GPa	25 (non-elastic)
PLGA (50/50)	1.47–1.61		0.7–7 GPa	7–20 (non-elastic)
POMC and POC	1.49–1.54	0.4	4.7–6.1 MPa	57–103
PEG hydrogels	1.35–1.47	0.17–25	1–44 kPa	300–2000
PAM hydrogels	1.46–1.50	1–11	20–27 MPa	13–74
PDMS	1.41–1.47	0.5	0.57–3.7 MPa	95–140
Polyurethane	1.46	2	0.3 MPa	10
COCE	1.51	4	34 MPa	230

Conclusion

In summary, our research demonstrates the viability of flexible organic crystals as effective and safe materials for delivering light in biological tissues. These crystals possess transparency, flexibility, and biocompatibility, offering advantages over conventional waveguide materials. Their mechanical flexibility and low toxicity make them well-suited for interfacing with soft tissues. Through experiments in tissue and live animal models, we

have shown their ability to transmit both active and passive light signals without toxicity. Overall, Organic crystals offer a promising platform for the development of next-generation optical waveguides and devices with enhanced functionality and biocompatibility. Future studies may focus on optimizing the optical and mechanical properties of organic crystals, as well as exploring their applications in specific biomedical contexts, to unlock their full potential in translational medicine.

Supporting Information

Supporting Information is available and includes supplementary Figures 1–12 and Tables 1–3, references and legends for the supplementary Movies S1 and S2.

Disclosures

All animal studies were performed according to the guidelines and the overall project protocols were approved by the Welfare and Ethics Committee of Laboratory Animal, College of Basic Medical Sciences, Jilin University.

Conflict of Interest

There are no conflicts to declare.

Funding Information

This work was supported by the National Natural Science Foundation of China (52173164 and 52373181), the Natural Science Foundation of Jilin Province (20230101038JC), and a fund from New York University Abu Dhabi. This material is based upon works supported by Tamkeen under NYUAD RRC Grant No. CG011.

References

1. Brümmer, F.; Pfannkuchen, M.; Baltz, A.; Hauser, T.; Thiel, V. Light inside sponges. *J. Exp. Marine. Biol. Ecol.* **2008**, *367*, 61–64.

2. Sundar, V. C.; Yablon, A. D.; Grazul, J. L.; Ilan, M.; Aizenberg J. Fibre-optical features of a glass sponge. *Nature* **2003**, *424*, 899–900.

3. Choi, M.; Humar, M.; Kim, S.; Yun, S.-H. Step-Index Optical Fiber Made of Biocompatible Hydrogels. *Adv. Mater.* **2015**, *27*, 4081–4086.

4. Jiang, Y.; Qi, W.; Zhang, Q.; Liu, H.; Zhang, J.; Du, N.; Nazempour, R.; Su, Y.; Fu, R.; Zhang, K.; Lyu, P.; Dong, F.; Yin, L.; Sheng, X.; Wang, Y. Green Light-Based Photobiomodulation with an Implantable and Biodegradable Fiber for Bone Regeneration. *Small Methods* **2020**, *4*, 1900879.

5. Deisseroth, K. Optogenetics, *Nat. Methods* **2011**, *8*, 26–29.

6. Bansal, A.; Yang, F.; Xi, T.; Zhang, Y.; Ho, J. S. In vivo wireless photonic photodynamic therapy. *Proc. Natl. Acad. Sci. USA* **2018**, *115*, 1469–1474.

7. Zhao, H.; O'Brien, K.; Li, S.; Shepherd, R. F. Optoelectronically innervated soft prosthetic hand via stretchable optical waveguides. *Sci. Robot.* **2016**, *1*, eaai7529.

8. Kelsey, A. P.; Amy, C. B.; Wade, K. S.; Jeffrey, R. C. Stab injury and device implantation within the brain results in inversely multiphasic neuroinflammatory and neurodegenerative responses. *J. Neural Eng.* **2012**, *9*, 046020.

9. George, C. M.; Howard, D. R.; Allan, I. L.; Claire-Ann, G.; Robert, E. G.; Ravi, V. B. Implanted neural electrodes cause chronic, local inflammation that is correlated with local neurodegeneration. *J. Neural Eng.* **2009**, *6*, 056003.

10. Guo, J.; Yang, C.; Dai, Q.; Kong, L. Soft and Stretchable Polymeric Optical Waveguide-Based Sensors for Wearable and Biomedical Applications. *Sensors* **2019**, *19*, 3771.

11. Shabahang, S.; Kim, S.; Yun, S.-H. Light-Guiding Biomaterials for Biomedical Applications. *Adv. Funct. Mater.* **2018**, *28*, 1706635.

12. Nazempour, R.; Zhang, Q.; Fu, R.; Sheng, X. Biocompatible and Implantable Optical Fibers and Waveguides for Biomedicine. *Materials* **2018**, *11*, 1283.

13. Liu, H.; Lu, Z.; Zhang, Z.; Wang, Y.; Zhang, H. Highly Elastic Organic Crystals for Flexible Optical Waveguides. *Angew. Chem. Int. Ed.* **2018**, *57*, 8448–8452.

14. Catalano, L.; Karothu, D. P.; Schramm, S.; Ahmed, E.; Rezgui, R.; Barber, T. J.; Famulari, A.; Naumov, P. Dual-Mode Light Transduction through a Plastically Bendable Organic Crystal as an Optical Waveguide. *Angew. Chem. Int. Ed.* **2018**, *57*, 17254–17258.

15. Hayashi, S.; Yamamoto, S.; Takeuchi, D.; Ie, Y.; Takagi, K. Creating Elastic Organic Crystals of π-Conjugated Molecules with Bending Mechanofluorochromism and Flexible Optical Waveguide. *Angew. Chem. Int. Ed.* **2018**, *57*, 17002–17008.

16. Zhuo, M.; Tao, Y.; Wang, X.; Wu, Y.; Chen, S.; Liao, L.; Jiang, L. 2D Organic Photonics: An Asymmetric Optical Waveguide in Self-Assembled Halogen-Bonded Cocrystals. *Angew. Chem. Int. Ed.* **2018**, *57*, 11300–11304.

17. Li, Y.; Ma, Z.; Li, A.; Xu, W.; Wang, Y.; Jiang, H.; Wang, K.; Zhao, Y.; Jia, X. A Single Crystal with Multiple Functions of Optical Waveguide, Aggregation-Induced Emission, and Mechanochromism. *ACS Appl. Mater. Interfaces* **2017**, *9*, 8910–8918.

18. Annadhasan, M.; Karothu, D. P.; Chinnasamy, R.; Catalano, L.; Ahmed, E.; Ghosh, S.; Naumov, P.; Chandrasekar, R. Micromanipulation of Mechanically Compliant Organic Single-Crystal Optical Microwaveguides. *Angew. Chem. Int. Ed.* **2020**, *59*, 13821–13830.

19. Karothu, D. P.; Dushaq, G.; Ahmed, E.; Catalano, L.; Polavaram, S.; Ferreira, R.; Li, L.; Mohamed, S.; Rasras, M.; Naumov, P. Mechanically robust amino acid crystals as fiber-optic transducers and wide bandpass filters for optical communication in the near-infrared. *Nat. Commun*. **2021**, *12*, 1326.

20. Guerin, S.; Stapleton, A.; Chovan, D.; Mouras, R.; Gleeson, M.; McKeown, C.; Noor, M. R.; Silien, C.; Rhen, F. M. F.; Kholkin, A. L.; Liu, N.; Soulimane, T.; Tofail S. A. M.; Thompson D. Control of piezoelectricity in amino acids by supramolecular packing. *Nat. Mater.* **2018**, *17*, 180–186.

21. Naumov, P.; Karothu, D. P.; Ahmed, E.; Catalano, L.; Commins, P.; Halabi, J. M.; Al-Handawi, M. B.; Li, L. Artificial Chloride-Selective Channel: Shape and Function Mimic of the ClC Channel Selective Pore. *J. Am. Chem. Soc.* **2020**, *142*, 13273–13277.

22. Ahmed, E.; Karothu, D. P.; Naumov, P. Crystal Adaptronics: Mechanically Reconfigurable Elastic and Superelastic Molecular Crystals. *Angew. Chem. Int. Ed***. 2018**, *57*, 8837–8846.

23. Thompson, A. J.; Orué, A. I. C.; Nair, A. J.; Price, J. R.; McMurtrie, J. C.; Clegg J. K. Elastically flexible molecular crystals. *Chem. Soc. Rev.* **2021**, *50*, 11725–11740.

24. Worthy, A.; Grosjean, A.; Pfrunder, M. C.; Xu, Y.; Yan, C.; Edwards, G.; Clegg J. K.; McMurtrie, J. C. Atomic resolution of structural changes in elastic crystals of copper(II) acetylacetonate. *Nat. Chem.* **2018**, *10*, 65–69.

25. Lan, L.; Yang, X.; Tang, B.; Yu, X.; Liu, X.; Li, L.; Naumov, P.; Zhang, H. Hybrid Elastic Organic Crystals that Respond to Aerial Humidity. *Angew. Chem. Int. Ed.* **2022**, *61*, e202200196.

26. Mishra, M. K.; Kadambi, S. B.; Ramamurty, U.; Ghosh, S. Elastic flexibility tuning via interaction factor modulation in molecular crystals. *Chem. Commun.* **2018**, *54*, 9047–9050.

27. Lan, L.; Liu, H.; Yu, X.; Liu, X.; Zhang, H. Polymer-Coated Organic Crystals with Solvent-Resistant Capacity and Optical Waveguiding Function. *Angew. Chem. Int. Ed.* **2021**, *60*, 11283–11287.

28. Li, Z. Z.; Wu, J. J.; Wang, X. D.; Wang, K. L.; Zhang, S.; Xie, W. F.; Liao, L. S. Controllable Fabrication of In-Series Organic Heterostructures for Optical Waveguide Application. *Adv. Opt. Mater.* **2019**, *7*, 1900373.

29. Li, Y.; Ma, Z.; Li, A.; Xu, W.; Wang, Y.; Jiang, H.; Wang, K.; Zhao, Y.; Jia, X. A Single Crystal with Multiple Functions of Optical Waveguide, Aggregation-Induced Emission, and Mechanochromism. *ACS Appl. Mater. Interfaces* **2017**, *9*, 8910–8918.

30. Thompson, A. J.; Powell, J. A.; Melville, J. N.; McMurtrie, J. C.; Clegg, J. K. Crystals of Aliphatic Derivatives of [Cu(acac)2] have Distinct Atomic-Scale Mechanisms of Bending. *Small* **2023**, *19*, 2207431.

31. Min, S.; Dhamsaniya, A.; Zhang, L.; Hou, G.; Huang, Z.; Pambhar, K.; Shah, A. K.; Mehta, V. P.; Liu, Z.; Song, B. Scale Effect of a Fluorescent Waveguide in Organic Micromaterials: A Case Study Based on Coumarin Microfibers. *J. Phys. Chem. Lett.* **2019**, *10*, 5997–6002.

32. Shi, Y.-L.; Wang, X.-D. 1D Organic Micro/Nanostructures for Photonics, *Adv. Funct. Mater.* **2021**, *31*, 2008149.

33. Shi, Y.-L.; Zhuo, M.-P.; Wang, X.-D.; Liao, L.-S. Two-Dimensional Organic Semiconductor Crystals for Photonics Applications. *ACS Appl. Nano Mater.* **2020**, *3*, 1080–1097.

34. Wu, S.; Zhou, B.; Yan, D. Recent Advances on Molecular Crystalline Luminescent Materials for Optical Waveguides. *Adv. Opt. Mater.* **2021**, *9*, 2001768.

35. Catalano, L.; Commins, P.; Schramm, S.; Karothu, D. P.; Rezgui, R.; Hadef, K.; Naumov, P. A filled organic crystal as a hybrid large-bandwidth optical waveguide. *Chem. Commun.* **2019**, *55*, 4921–4924.

36. Tian, D.; Chen, Y. Optical Waveguides in Organic Crystals of Polycyclic Arenes. *Adv. Opt. Mater.* **2021**, *9*, 2002264.

37. Pejov, L.; Panda, M. K.; Moriwaki, T.; Naumov, P. Probing Structural Perturbation in a Bent Molecular Crystal with Synchrotron Infrared Microspectroscopy and Periodic Density Functional Theory Calculations. *J. Am. Chem. Soc*. **2017**, *139*, 2318–2328.

38. Ahmed, E.; Karothu, D. P.; Warren, M.; Naumov, P. Shape-memory effects in molecular crystals. *Nat. Commun.* **2019**, *10*, 3723.

39. Commins, P.; Hara, H.; Naumov, P. Self-Healing Molecular Crystals. *Angew. Chem. Int. Ed*. **2016**, *55*, 13028–13032.

40. Colin-Molina, A.; Karothu, D. P.; Jellen, M. J.; Toscano, R. A.; Garcia-Garibay, M. A.; Naumov, P.; Rodríguez-Molina, B. Thermosalient Amphidynamic Molecular Machines: Motion at the Molecular and Macroscopic Scales. *Matter* **2019**, *1*, 1033–1046.

41. Sahoo, S. C.; Nath, N. K.; Zhang, L.; Semreen, M. H.; Al-Tel, T. H.; Naumov, P. Actuation based on thermo/photosalient effect: a biogenic smart hybrid driven by light and heat. *RSC Adv.* **2014**, *4*, 7640–7647.

42. Commins, P.; Natarajan, A.; Tsai, C.-K.; Khan, S. I.; Nath, N. K.; Naumov, P.; Garcia-Garibay, M. A. Structure–Reactivity Correlations and Mechanistic Understanding of the Photorearrangement and Photosalient Effect of α-Santonin and Its Derivatives in Solutions, Crystals, and Nanocrystalline Suspensions. *Cryst. Growth Des*. **2015**, *15*, 1983–1990.

43. Panda, M. K.; Centore, R.; Causa, M.; Tuzi, A.; Borbone, F.; Naumov, P. Strong and Anomalous Thermal Expansion Precedes the Thermosalient Effect in Dynamic Molecular Crystals. *Sci. Rep.* **2016**, *6*, 29610.

44. Khalil, A.; Ahmed, E.; Naumov, P. Metal-coated thermosalient crystals as electrical fuses. *Chem. Commun*. **2017**, *53*, 8470–8473.

45. Catalano, L.; Berthaud, J.; Dushaq, G.; Karothu, D. P.; Rezgui, R.; Rasras, M.; Ferlay, S.; Hosseini, M. W.; Naumov, P. Sequencing and Welding of Molecular Single-Crystal Optical Waveguides. *Adv. Funct. Mater.* **2020**, *30*, 2003443.

46. Venkatakrishnarao, D.; Mohiddon, M. A.; Chandrasekhar, N.; Chandrasekar, R. Photonic Microrods Composed of Photoswitchable Molecules: Erasable Heterostructure Waveguides for Tunable Optical Modulation. *Adv. Opt. Mater.* **2015**, *3*, 1035–1040.

47. Halabi, J. M.; Ahmed, E.; Catalano, L.; Karothu, D. P.; Rezgui, R.; Naumov, P. Spatial Photocontrol of the Optical Output from an Organic Crystal Waveguide. *J. Am. Chem. Soc.* **2019**, *141*, 14966–14970.

48. Apter, B.; Lapshina, N.; Handelman, A.; Fainberg, B. D.; Rosenman, G. Peptide Nanophotonics: From Optical Waveguiding to Precise Medicine and Multifunctional Biochips. *Small* **2018**, *14*, 1801147.

49. Ji, W.; Xue, B.; Arnon, Z. A.; Yuan, H.; Bera, S.; Li, Q.; Zaguri, D.; Reynolds, N. P.; Li, H.; Chen, Y.; Gilead, S.; Rencus-Lazar, S.; Li, J.; Yang, R.; Cao, Y.; Gazit E. Rigid Tightly Packed Amino Acid Crystals as Functional Supramolecular Materials. *ACS Nano* **2019**, *13*, 14477–14485.

50. Venkatakrishnarao, D.; Sahoo, C.; Mamonov, E. A.; Novikov, V. B.; Mitetelo, N. V.; Naraharisetty, S. R. G.; Murzina, T. V.; Chandrasekar, R. Chiral organic photonics: self-assembled micro-resonators for an enhanced circular dichroism effect in the non-linear optical signal. *J. Mater. Chem. C* **2017**, *5*, 12349–12353.

51. Mitetelo, N.; Venkatakrishnarao, D.; Ravi, J.; Popov, M.; Mamonov, E.; Murzina, T. V.; Chandrasekar, R. Chirality-Controlled Multiphoton Luminescence and Second-Harmonic Generation from Enantiomeric Organic Micro-Optical Waveguides. *Adv. Opt. Mater.* **2019**, *7*, 1801775.

52. Wei, G.-Q.; Wang, X.-D.; Liao, L.-S. Recent Advances in 1D Organic Solid-State Lasers. *Adv. Funct. Mater.* **2019**, *29*, 1902981.

53. Chandrasekar, R. Organic photonics: prospective nano/micro scale passive organic optical waveguides obtained from π-conjugated ligand molecules. *Phys. Chem. Chem. Phys.* **2014**, *16*, 7173–7183.

54. Chu, X.; Lu, Z.; Tang, B.; Liu, B.; Ye, K.; Zhang, H. Engineering Mechanical Compliance of an Organic Compound toward Flexible Crystal Lasing Media. *J. Phys. Chem. Lett.* **2020**, *11*, 5433–5438.

55. Yao, W.; Yan, Y.; Xue, L.; Zhang, C.; Li, G.; Zheng, Q.; Zhao, Y. S.; Jiang, H.; Yao, J. Controlling the Structures and Photonic Properties of Organic Nanomaterials by Molecular Design. *Angew. Chem. Int. Ed.* **2013**, *52*, 8713–8717.

56. Karothu, D. P.; Halabi, J. M.; Ahmed, E.; Ferreira, R.; Spackman, P. R.; Spackman, M. A.; Naumov, P. Global Analysis of the Mechanical Properties of Organic Crystals. *Angew. Chem. Int. Ed.* **2022**, *134*, e202113988.

57. Mondal, A.; Bhattacharya, B.; Das, S.; Bhunia, S.; Chowdhury, R.; Dey, S.; Reddy, C. M. Metal-like Ductility in Organic Plastic Crystals: Role of Molecular Shape and Dihydrogen Bonding Interactions in Aminoboranes. *Angew. Chem. Int. Ed.* **2020**, *59*, 10971–10980.

58. Spackman, P. R.; Grosjean, A.; Thomas, S. P.; Karothu, D. P.; Naumov, P.; Spackman, M. A. Quantifying Mechanical Properties of Molecular Crystals: A Critical Overview of Experimental Elastic Tensors. *Angew. Chem. Int. Ed.* **2022**, *61*, e202110716.

Table of Contents Graphic (required)